DEADTIME CALIBRATION IN HIGH-RATE MICROSTRIP GAS COUNTERS

J.E.Bateman, D.M.Duxbury

Science and Technology Facilities Council, Rutherford Appleton Laboratory, Harwell Science and Innovation Campus, Didcot, Oxfordshire, OX11 0QX, U.K.

21 December 2009

Abstract

The advent of the Microstrip Gas Chamber (MSGC) has permitted the development of position-sensitive gas avalanche detectors which combine sub-millimeter spatial resolution with multi-MHz global rate capabilities not attainable with traditional types of gas counter. Based on massively parallel electronic readout, the need to keep down electronic channel costs imposes a simple front-end design without in-built deadtime compensation. In this report we show that in-situ calibration of the deadtime of the detector system is straight-forward and reliable. Methods are described for applications to x-ray and neutron detection.

1. Introduction

The advent of high intensity accelerator-based sources for materials studies such as DIAMOND [1] for x-rays and ISIS [2] for neutrons, combined with the ubiquity of digital electronics has created a demand for digital pulse, position sensitive detectors for the radiation patterns scattered from target samples. The HOTWAXS detector [3] is such a device. Based on microstrip gas chamber (MSGC) technology [4] it images x-ray diffraction patterns using 1024 sensitive strip detectors of average width ~450μm which point at the target sample. In the implementation used on DIAMOND two strips are coupled electrically resulting in 512 channels, each provided with independent preamplifier, shaping amplifier and discriminator, the output of which is fed into a frame memory which can record exposure sequences with time frames as short as 10μs. Figure 1 shows a typical scattering pattern – observed from a sample of high density polyethylene (HDPE) [5].

A comparable device is currently under development for imaging neutron diffraction patterns called OSMOND for the CRISP [6] instrument on ISIS with appropriate modifications for neutron detection. In order to explore the particular requirements for efficient neutron detection a development device named FASTGAS [7] was created with the aim of a fast-counting replacement for the standard single-wire proportional counter used for specular reflectometry measurements on the CRISP reflectometer. The FASTGAS detector consists of an MSGC plate with 8 groups of 10 sensitive strips each 300μm wide and 60mm long. Each group of strips is connected to a standard HOTWAXS electronic readout channel giving 8 parallel readouts covering the same width as the 1 inch diameter proportional counter in present use. The neutron results presented in this report were obtained from this detector.

The requirement to count at rates greater than 1MHz per channel (inevitably requiring deadtime correction) with simple electronics renders it desirable to avoid the need for a dedicated deadtime circuit for each channel. A possible answer to this problem is *in situ* calibration of the rate characteristics of the system based on the elementary deadtime model which generally describes the behaviour of electronic systems fed a random stream of input pulses. This report describes the implementation of this method to both x-ray and neutron detectors operating at data capture rates of ~1MHz per channel.

2. The Elementary Deadtime Model

Any electronic system takes a finite time to process an incident pulse during which any subsequent arrivals are ignored. This is the system deadtime. If a random (in time) stream of pulses is incident at a rate N_i (per second) the system will process a number N_o in a second with a loss of the events occurring in a period (expressed as a fraction of a second) $N_o\tau$. Thus:

$$N_o = N_i (1 - N_o\tau) \qquad (1)$$

This can be rearranged to give the useful formula for the through-put of the system:

$$N_o = N_i / (1 + N_i\tau) \qquad (2)$$

Re-arranging we can obtain the correcting function if τ is known:

$$N_i = N_o / (1 - N_o\tau) \qquad (3)$$

A final rearrangement which is useful in analysis is:

$$1/N_o = 1/N_i + \tau \qquad (4)$$

The above formulae are found to describe the behaviour of most simple counting systems over their range of valid operation. Departure from them usually results from non-linear overloading of some part of the preceding chain, be it the radiation counter or amplifier. In particular, equation (2) shows that at low rates ($N_i\tau \ll 1$) $N_o \approx N_i$, while the maximum output rate ($N_i\tau \gg 1$) is $1/\tau$, reached asymptotically with $N_o = N_i/2$ at $N_i\tau = 1$.

2.1 Series Deadtimes

Practical pulse counting systems consist of a chain of distinct electronic modules, each with its own deadtime. The above formulas provide a simple relation for the overall deadtime of the data acquisition as a function of the deadtimes of the individual components. Let us consider (for example) a chain consisting of three modules with deadtimes τ_1, τ_2, τ_3 before final storage of the event is achieved.

If the output rate of module 3 is N_{o3} and N_{i1} is the input to module 1 then we have using equation (4) above:

$$1/N_{o3} = 1/N_{i3} + \tau_3$$

However since $N_{i3} = N_{o2}$ we can replace the term $1/N_{i3}$ as follows:

$$1/N_{o3} = 1/N_{i2} + \tau_2 + \tau_3$$

Repeating this process using the fact that $N_{i2} = N_{o1}$ we find:

$$1/N_{o3} = 1/N_{i1} + \tau_1 + \tau_2 + \tau_3.$$

This process clearly generalises to the conclusion that in a series chain of modules the overall effective deadtime is given by the sum of the deadtimes of the individual modules: $\tau_{eff} = \sum \tau_i$.

2.2 Parallel Deadtimes

It is possible in some cases (in particular in the case of the MSGC which can easily subdivide the counting area) to provide parallel counting systems from which the data can be combined off-line. Equation (2) above enables us to estimate the benefit to be derived from parallel readout in such a case. For simplicity we consider a global rate N_i distributed into *m* identical channels with deadtime τ.

The input rate to each channel is now N_i/m and the final effective output rate is mN_{on} where n indexes the channels. From (2) we get:

$$N_{on} = N_i/m \, / \, \{1 + N_i\tau/m\}$$

Multiplying N_{on} by m to give the effective total rate:

$$N_{oeff} \; = \; N_i \, / \, \{ \, 1 + N_i(\tau/m)\}$$

In other words the effective deadtime of the system is $\tau_{eff} = \tau/m$. This maximum benefit of a parallel readout system will only occur in the (uninteresting) case of a uniform spatial distribution. However, most features of interest in a scattering spectrum are spread out over many channels and the benefit is real. Often there are regions of intense background that paralyse a global readout system. Deadtime effects (and corrections) are local in massively parallel readouts (such as HOTWAXS) permitting much enhanced capabilities in detecting weak features as well as allowing fast time framing.

3. Characterisation of some aspects of the Performance of the HOTXAXS Electronics

The counting chain which precedes the final data-capture system of any detector consists of several modules which, in the case of HOTWAXS comprise the detector itself (a single strip of MSGC), a charge-sensitive pre-amplifier, a shaping amplifier and a discriminator. The charge pre-amp and the shaping amplifier are incorporated in the detector housing. This is mandated by the high channel density (>2 channels/mm). The same feature also dictates the lack of electronic deadtime correction circuitry and the use of low voltage ($\pm5V$) rails to minimise cooling problems.

The characterisation of some deadtime properties requires a genuinely stochastic source of high rate events (i.e. beamline tests). However a key characteristic can be measured off-line using pulse generators. Figure 2 shows a CRT image of the pulse configuration used to estimate the Pulse Pair Resolution (PPR) of the electronics. Two units (Tektronix 508 Pulse Generators) generating step charge pulses through a 1pF test capacitor are slaved together and the delay between them reduced until the second pulse is lost. In a more elaborate design this delay (the PPR) would be forced to be constant but in this design it is controlled largely by the interaction of the shaped analogue pulse width and the discriminator threshold. Figure 3 shows the measured PPR as a function of the ratio of the pulse peak height (PPH) to the discriminator level (LLD). Also shown, for reference is the PPR estimated from the time of an idealised pulse waveform above threshold. (The charge delivery from the detector is not an infinitely sharp step function so the idealised response is only an approximation). The measured PPR was not found to depend significantly on the amplitude of the slave pulse over a typical dynamic range so the data in figure 3 is an average over a range of slave pulse amplitudes.

The discriminators are generally housed with the remote data capture system and vary. However, set to deliver a 50ns output pulse their properties play a negligible role in determining the front-end deadtime.

The dynamic range of the PPH/LLD ratio rarely exceeds 10 in practical applications in both x-ray and neutron counting so that the estimated deadtime of these circuits always lies below 200ns. As will appear below, the mathematical deadtime model operates quite happily with an *average* deadtime and the value observed in any practical situation is a weighted average over the pulse height spectrum present in the given exposure. The overall deadtime observed in data acquisition is (as noted in Section 2.1 above) the sum of this deadtime plus that of the data capture system itself.

4. Deadtime Calibration in X-ray Applications

It is clear from the results of Section 3 that the system deadtime in any experimental situation depends on many parameters intrinsic to the situation, viz: the beam energy, the counter gas gain, the discriminator settings, etc. Thus the calibration process must be self-contained with all the parameters as set for the experimental exposure. Equation (2) indicates the basis for this process by showing that $N_o \approx N_i$ when $N_i\tau \ll 1$. The basis of the standard method is thus to calibrate a series of x-ray attenuators (metal foils) at low rates using the detector itself. On removing these calibrated foils from the beam the true values of N_i at higher rates can be calculated to provide the abscissa values for the plot of N_o vs N_i before fitting equation (2).

A variant of this approach can be seen in figure 4 where a series of identical foils are used to attenuate the beam impinging on the sample irradiated in figure 1. The peak channel counts (rates) of different (bragg) orders of scattering give a series of curves of N_o vs the number of foils (n) with the expected negative exponential form evident. It is important that sufficient statistics are taken so that an accurate fit to a negative exponential (linear in the logarithmic plot) using only the lowest rate data points to satisfy the condition $N_i\tau \ll 1$. It is also important that the attenuators are placed well upstream of the detector to avoid contamination of the low rate data by background and leakage (fluorescence, etc.) from the foils.

When the low rate fits in figure 4 are extrapolated back to high rates, the loss of counts from the deadtime becomes clear at the highest rates. The fits can now be used to provide N_i in the plot of N_o vs N_i shown in figure 5 where the data from the peak channels of the 3 orders of scattering in figure 1 are used. A fit of equation (2) now delivers the overall deadtime of the whole system (including data capture).

An iterative process can be used to check that the measured deadtime value is stable by using the τ value obtained to obtain an estimated N_i vs n curve using equation (3). Fitting the attenuation function to the bottom end of this curve is in principle even more accurate than before and the subsequent re-estimate of τ more accurate. The quality of the data in figure 4 is so high that this iteration provides exactly the same value of τ as the first loop leading to confidence in the result. If the low rate data is noisy or corrupt the iterative process can take 2 or 3 passes for the value of τ to stabilise.

The precise value of τ derived from figure 5 (357ns or 335ns) depends on how far up the data curve the fit is taken. This is a result of the onset of non-linear processes in the detector and pre-amplifier which are discussed below. The rate values used in figures 4 and 5 are taken from the peak channels of the 3 orders of scattering in the data set of figure 1. The deadtime values are specific to a channel; however the conformity of the three data sets in figure 5 shows that there is no significant variation in the deadtime as a function of channel position and the same correction process can be applied (using equation (3)) to all channels. The continuous curve in figure 2 shows the deadtime-corrected spectrum.

5. Deadtime Calibration in Neutron Applications

The calibrated attenuator used in Section 4 above for x-rays can equally well be applied to evaluating the deadtime performance of a neutron-sensitive detector. In reference [8] is to be found an example of such a deadtime calibration applied to a 2-D imaging neutron MSGC. For the examination of the rate performance of the FASTGAS detector an alternative method was used. This method utilises the range of rates present in the Maxwellian time-of-flight (TOF) spectrum observed during a typical 20ms time frame on an ISIS beam line. For these tests the digital outputs (i.e. after the discriminator) of 7 sections of FASTGAS (each of 10 strips) were recorded in a single channel of the ISIS Digital Acquisition Electronics (DAE) [9] system.

The pulse rate of the detector was varied by controlling the CRISP beamline collimator slits. Figure 6 shows the TOF spectra obtained from FASTGAS in 10 000 frame exposures as the slits were varied from 0.2mm to 8mm. The peak of the Maxwellian provides a convenient diagnostic of the onset of deadtime effects. If we assume that the detector is still comfortably in the proportional range with one of the narrow slits (e.g. 0.5mm) then dividing the section of spectrum under the peak in all the higher rate cases should give a straight line until deadtime effects set in over the peak at the higher rates. Figure 7 illustrates these results over the TOF range of 5000µs to 7300µs and as expected, at the largest slit settings a pronounced dip is seen in the ratio curves.

If the 0.5mm slit data is assumed to be in the rate-proportional region then we can say that it is proportional to N_i and so the ordinate of a ratio plot is just $N_o/\alpha N_i$. If we now plot the ordinate for a given slit ratio curve against the corresponding observed rate in that time bin at the given slit setting (i.e. the value from figure 6 divided by 10 000), then we have a plot of $N_o/\alpha N_i$ vs N_o. Equation (3) shows that this curve should fit the function $1 - N_o\tau$. Figure 8 shows these plots for the 5mm, 6mm, 7mm and 8mm data. Reasonable straight line fits are obtained but the slopes (τ) consistently decrease with the slit width. On reflection this is eminently reasonable as the plot must become absolutely flat when the 0.5mm data is divided by itself. Clearly the divisor is nearest to proportionality to the true input rate when α is very large i.e. $1/\alpha \rightarrow 0$. In figure 9 the "deadtime" measured from each of the fits in figure 8 are plotted against $1/\alpha$. Extrapolation to $1/\alpha = 0$ gives the "true" deadtime $\tau = 0.312$µs. The linear nature of the plot in figure 9 gives confidence in the method.

This method has the advantage of being entirely self-contained with just control of the beam intensity required. As always it is important to ensure good

statistical accuracy in the denominator (i.e. low rate) TOF spectrum. (A deadtime of 6.6μs was obtained by this method from much noisier data for the single wire proportional counter installed on the beamline.) A fast (100MHz) scaler counting the FASTGAS pulses from 7 sections in parallel permits an estimate to be made of the separate contributions of the detector electronics and the DAE. We can use the observed global scaler rates to estimate the rate corresponding to a TOF channel. (We note that the scaler rate contains 50 frames of 20000 time channels and figure 6 allows us to show that the mean rate in the 5000 - 7300μs window is 2.52 times the global mean). In figure 10 the DAE capture rate is plotted against the channel rate estimated from the scaler. In order to make the data fit the DAE deadtime of 0.312μs a deadtime of 0.184μs must be assumed for the 7-section counter-scaler system. The specific DAE contribution to the deadtime can be estimated at 312 – 184 = 124ns. Thus it can be concluded that in this 7-section configuration the counter and data collection deadtimes are well matched.

Figure 11 illustrates the effect on the TOF spectrum of the application of the deadtime correction (equation (3)) to the 8mm slit exposure in figure 6

6. Discussion

Beyond the clear conclusion that calibration and off-line deadtime correction is practicable, several interesting features emerge from the results presented above:

6.1 Non-Linearity at High Rates

It is clear from figures 5 and 10 that in both cases (HOTWAXS and FASTGAS) the measured rate begins to droop below the fitted deadtime curve at input rates approaching 2MHz. Such an effect arises from either (or both) gain saturation effects in the counter or the analogue electronics.

Extensive studies on MSGCs [10] showed that with pulses of the amplitude used in these devices (~2x10^5 electrons) rate densities on the plate of 1MHz/mm^2 could be sustained with minimal gain loss due to space charge effects. Our experience with the particular glass used in these devices (Schott S8900) puts this limit lower at about 200kHz/mm^2. In HOTWAXS the area of a strip is ~22.5mm^2 putting the limit for uniform irradiation at ~4.5MHz. Since the end of the strip nearer the target is more heavily loaded it is quite likely that some gain loss is beginning to be experienced at a 2MHz input rate.

In the FASTGAS case the 8mm slit beam covers ~168mm^2 giving a large factor of leeway as regards space charge effects in the counter so the departure from the fit in figure 10 directs attention to the analogue electronics. (It is important to recall that the calibration of the input rate scale in figure 10 is indirect and therefore slightly suspect). At very high rates the charge preamplifier can run out of headroom. Calculation shows that with the maximum signals from FASTGAS (1.55x10^5 electrons) the preamp output would move (on average) by 0.25V/MHz. With the 5V power rails this would not be expected to cause pulse saturation much below ~3V or 12MHz. Another possible cause is the small (~1%) negative undershoot which follows the shaped analogue pulse for several microseconds. At MHz rates following

pulses are pulled down slightly causing an effective gain reduction. However, since there are 7 channels combined after the discriminators making the data of figure 10, the rate in an individual analogue channel is only ~0.25MHz when the non-linearity begins to appear. Electronic problems at this rate are inconsistent with the behaviour of the same circuits in HOTWAXS. The source of the non-linearity in this data is thus unresolved.

Whatever the precise causes of the high rate non-linearity, it is small at the target rate of both systems, namely 2MHz incident with 1MHz capture. As figures 10 and 12 show, the non-linear portion of the rate response curve can be very satisfactorily modelled by modifying the simple deadtime constant to include a small rate-dependent term i.e. $\tau = \tau_0 + \alpha N_i$ where α is a small constant.

6.2 Deadtime Correction

The clear purpose of the deadtime calibration process is to permit the generation of "true" rate spectra from the detectors by off-line application of the derived algorithms. In the case of the simple (linear) correction, equation (3) is used with the single derived constant τ. In figure 12 the square symbols show the corrected estimate for the "true" rates using this method. The desired result is a line with slope unity implying that $N_o(corrected) = N_i$. Obviously the correction fails at the highest rates and recourse must be had to the non-linear fit described above.

Substituting $\tau = \tau_0 + \alpha N_i$ in equation (2) and rearranging, one can derive the equation:

$$\alpha N_i^2 + N_i (\tau_0 - 1/N_o) + 1 = 0 \qquad (5)$$

This is a simple quadratic equation with solution:

$$N_i = \{ (1/N_o - \tau_0) - \sqrt{[(\tau_0 - 1/N_o)^2 - 4\alpha]} \} / 2\alpha \qquad (6)$$

The minus sign before the square root is chosen to fulfil the necessary condition that equation (6) becomes equation (2) in the limit of α approaching zero.

In figure 12 is seen the result of applying the transformation of equation (6) to the measured rates of figure 5. The fit to the corrected data gives a slope of 0.99934 showing that the aim of fully correcting the rates over the whole range is satisfactorily achieved.

6.3 Deadtime Calibration Accuracy

Figure 13 presents the (fractional) residuals of the fit (y = x) to the HOTWAXS rates presented in figure 12 which have been corrected using equation (6). In the residuals three distinct groupings are evident, obviously corresponding to the data sets taken from three separate channels. The lowest rate data is noisiest due to poorer statistics and a possible small background. The means of the sets vary by order of a percent or two. This is consistent with the channel to channel errors inherent in the design [3]. The overall error is 1.25%.

Since the deadtime of the simple circuits is not electronically set it is a function of the pulse height for each incident pulse. The measured deadtime is thus a weighted average over the pulse height spectrum delivered by the detector. For neutrons (with a fixed converter gas) this does not change with neutron energy after the detector bias potentials are set. On the other hand, x-ray beams can easily be tuned to different energies with a consequent change in the pulse height spectrum and a shift in the deadtime. Thus a calibration procedure must be carried out for each beam energy if accurate deadtime correction is required.

While the attenuator method described in Section 4 above is superior to the method applied in Section 5 (figures 6 – 9), in that the onset of non-linearity can be detected explicitly, the application of the second method to x-ray detection could be advantageous in that only control of the beam intensity via the collimator slits is required and this is generally a readily accessible function. Clearly a smoothly varying scattering distribution is required for this method which would require a liquid or gas target rather than a solid one (to avoid Bragg peaks). A further requirement of this method is that the process used to control the beam intensity does not change the energy distribution within it, otherwise the spectral change will not just be due to the rate effects.

7. Conclusions

Multi-channel MSGC counting systems for x-rays and neutrons operating at MHz rates require deadtime correction. For massively parallel readout the front-end electronics must be made simple for reasons of space, heat dissipation and cost making the standard approach to deadtime correction unattractive. This report demonstrates that the simple standard deadtime model makes calibration of the variable average system deadtime a straight-forward operation with consistent results which can be applied off-line to experimental data. Two methods have been described. The explicit beam attenuator method (section 4) is more labour intensive but provides evidence of the onset of detector/front-end non-linearity explicitly. The normalised spectrum method (section 5) requires only control of the beam intensity by means of the beam collimators with analysis off-line. The method preferred will depend on the experimental circumstances.

References

1. http://www.diamond.ac.uk/Home.html

2. http://www.isis.rl.ac.uk/

3. J.E.Bateman[a], G.E.Derbyshire[a,b],G.Diakun[c],D.M.Duxbury[a],P.A.Fairclough[d], I.Harvey[c], W.I.Helsby[c], J.D.Lipp[a], A.S.Marsh[a], J.Salisbury[a], G.Sankar[e], E.J.Spill[a], R.Stephenson[a] and N.J.Terrill[b] , Nucl. Instr. & Meth. A580 (2007) 1526

4. A. Oed, Nucl. Instr. & Meth. A261 (1988) 351

5. J. E. Bateman, G. E. Derbyshire, G. Diakun, D. M. Duxbury, J. P. A. Fairclough, I. Harvey, W. I. Helsby, S-M Mai, O. O. Mykhaylyk, G. Sankar, E. J. Spill and R. Stephenson, IEEE Trans. Nucl. Sci. 55 (2), 729 (2008)

6. J. Penfold, R.C. Ward and W.G. Williams, J. Phys. E: Sci. Instrum. **20** (1987) 1411

7. J.E.Bateman, R. Dalgliesh, D.M.Duxbury, S.A.Holt, D. McPhail,   A.S.Marsh, N.J.Rhodes, E.M.Schooneveld, E.J.Spill and R.Stephenson, Rutherford Appleton Laboratory Report, RAL-TR-2009-012

8. J.E.Bateman, G.E.Derbyshire, D.M.Duxbury, A.S.Marsh, N.J.Rhodes, E.M.Schooneveld, E.J.Spill and R.Stephenson, IEEE Trans. Nucl. Sci. 52 (5), 1693 (2005)

9. S. Quinton, M. Johnson, J. Norris, W. Pulford and M. Watt, IEEE Trans. Nucl. Sci. 37 (6), 2156 (1990)

10. R. Bouclier, M. Capeans, G. Manzin, G. Million, L. Ropelewski, F. Sauli, L.I. Shekhtman, T. Temmel, G. Della Mea, G. Maggioni and V. Rigato, CERN Report, CERN-PPE/95-37
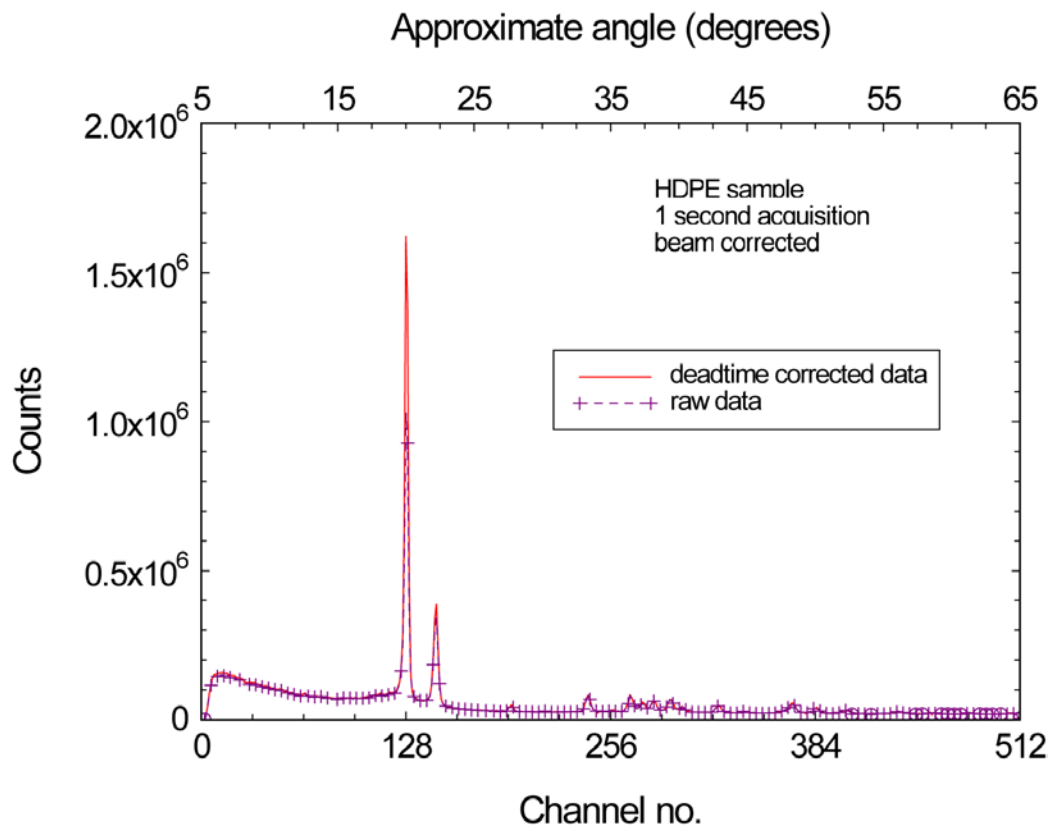
Figure 1. The scattering spectrum used to calibrate the HOTWAXS system deadtime
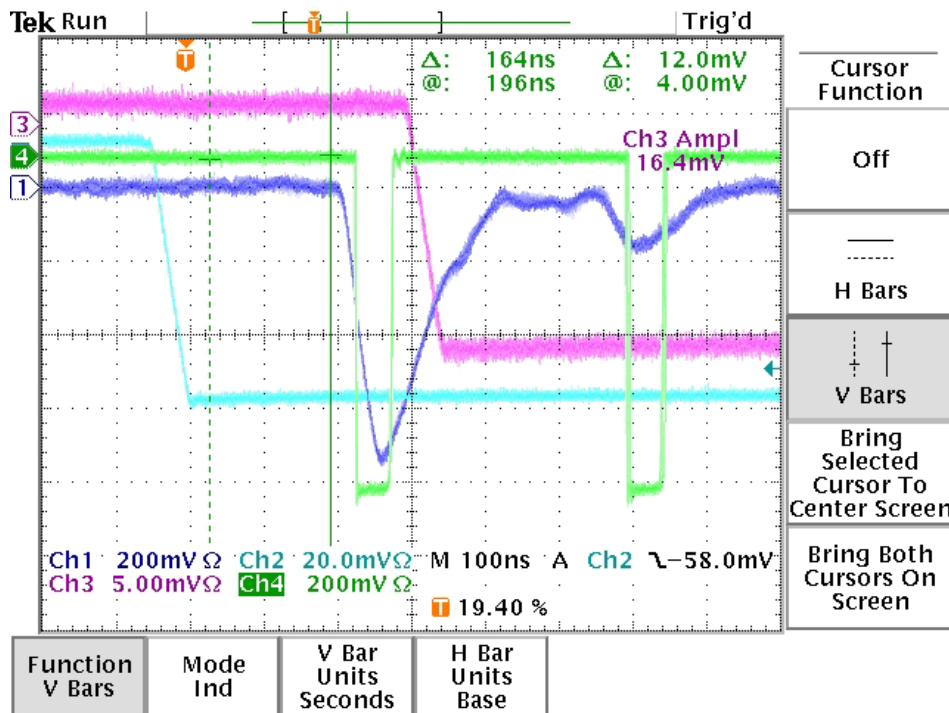
Figure 2. CRT traces of the input and output pulses in the PPR test set-up
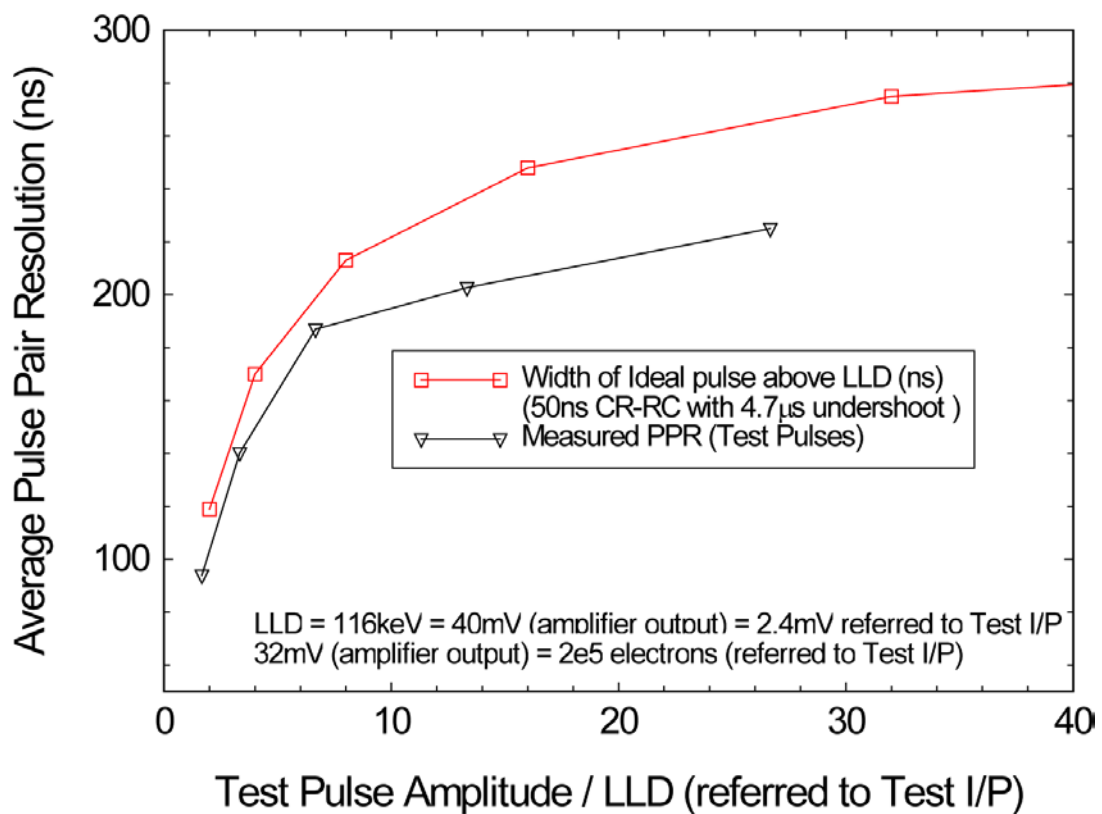
Figure 3. The measured PPR as a function of the pulse height dynamic ratio selected
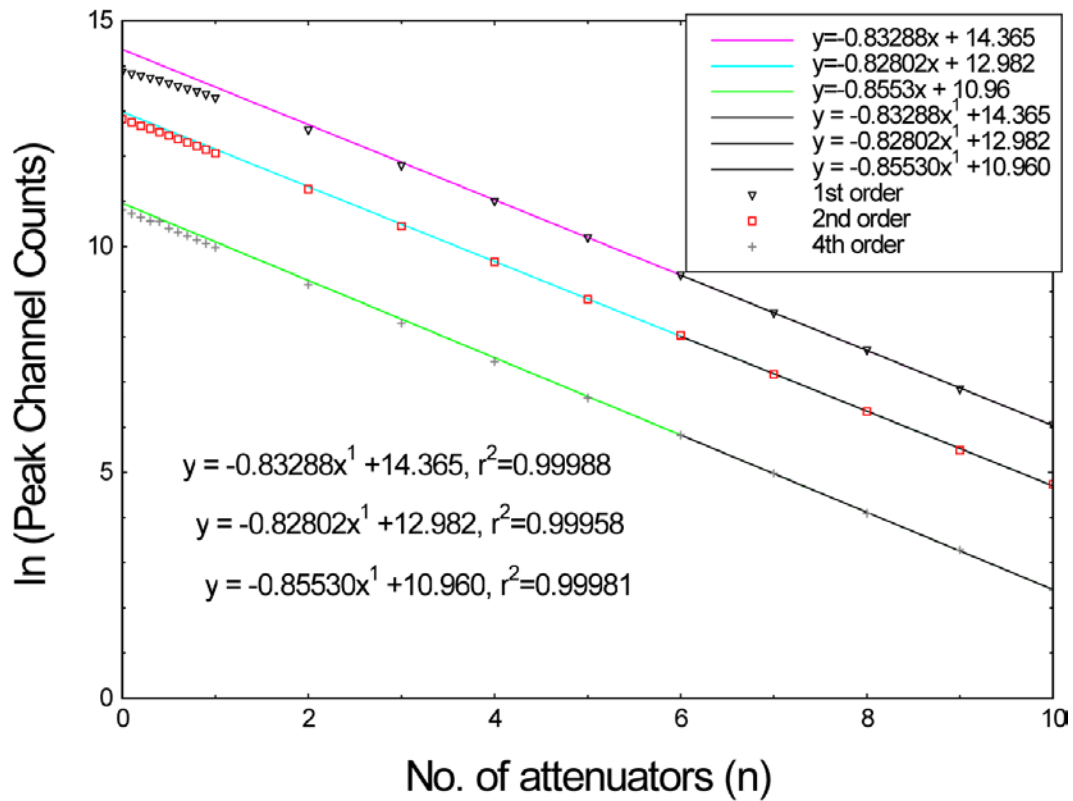
Figure 4. Plot of the counts (i.e. rates) in the peak channels of Fig. 1 as the beam is attenuated
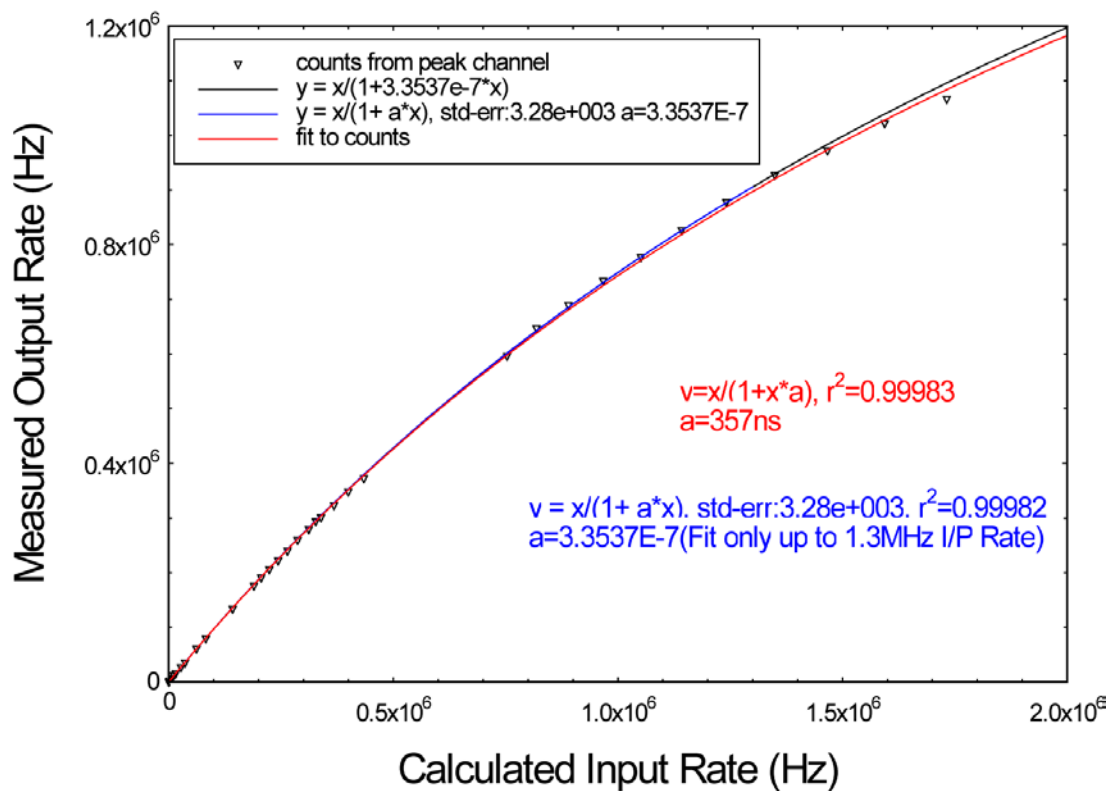
Figure 5. Standard deadtime curves derived from the data of figure 4
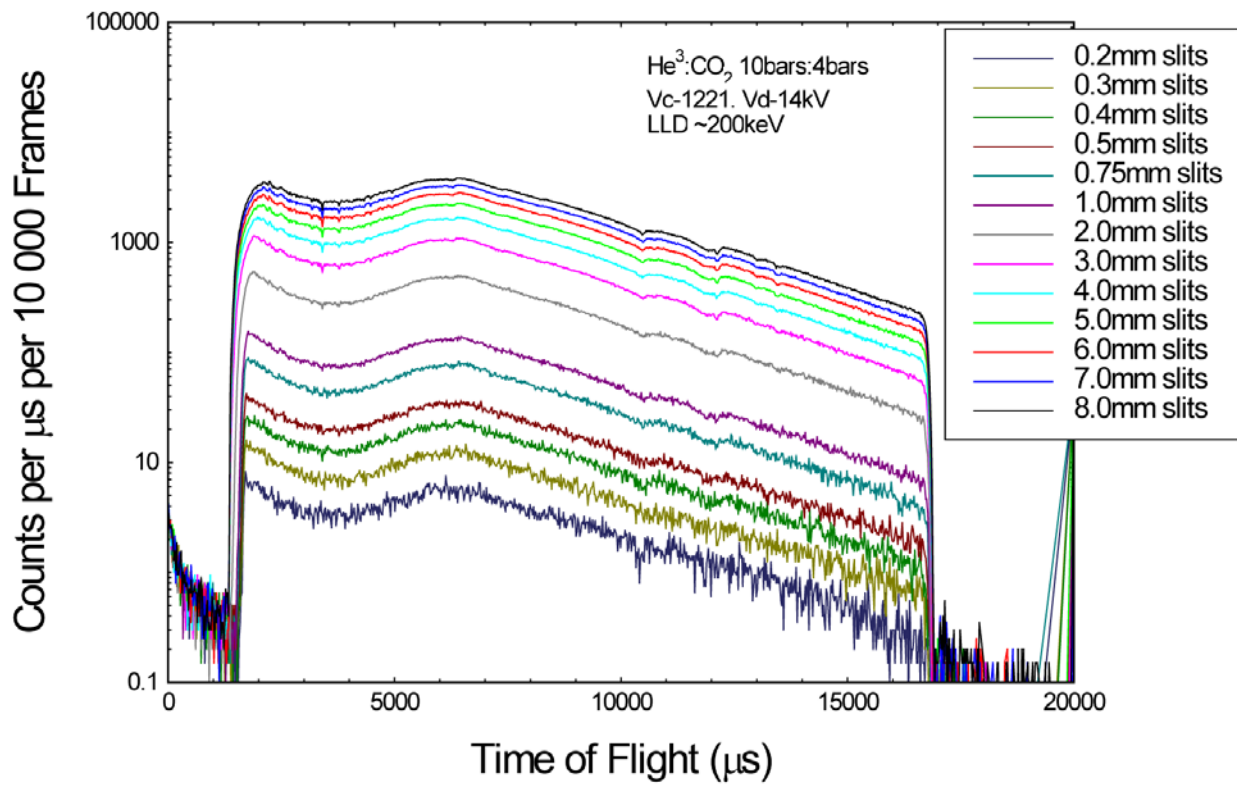
Figure 6. The neutron TOF spectra observed in FASTGAS with variable beam slits
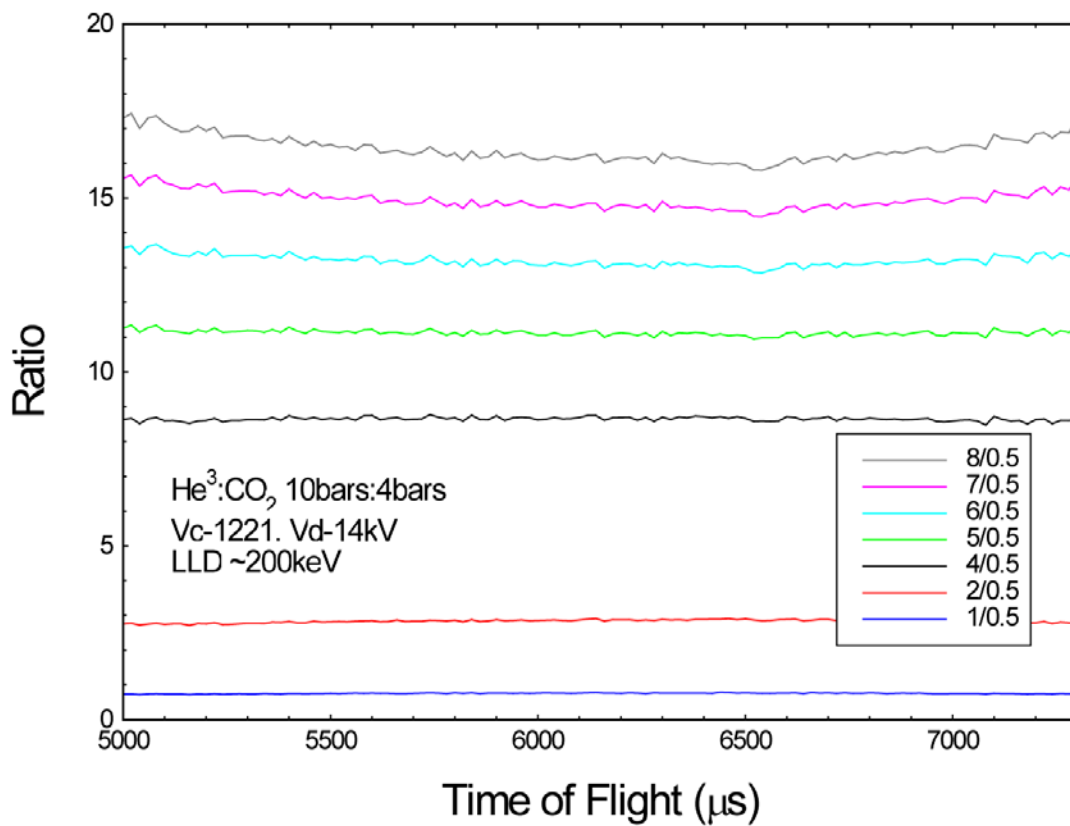

Figure 7. The "peak" sections of the ratio curves derived from the data of Figure 6
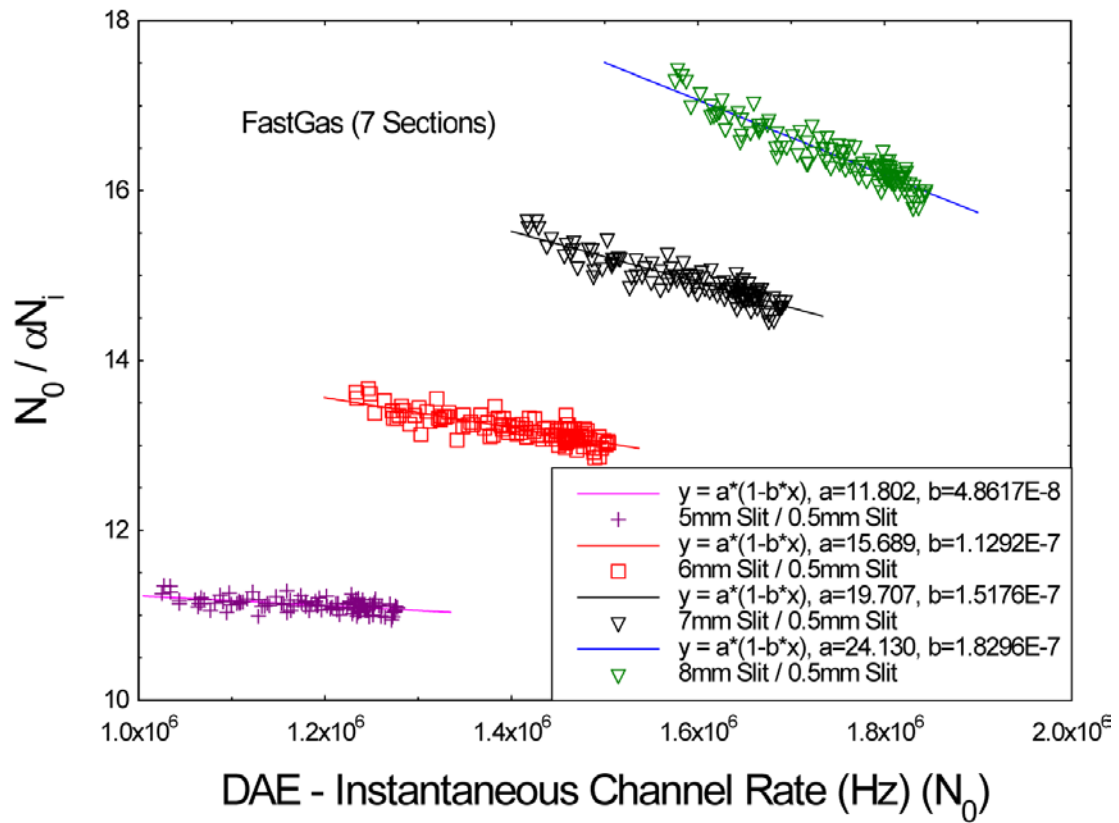
Figure 8. Plot of the ratio data of Fig. 7 against the corresponding time channel rate of Fig. 6 for the four highest slit widths
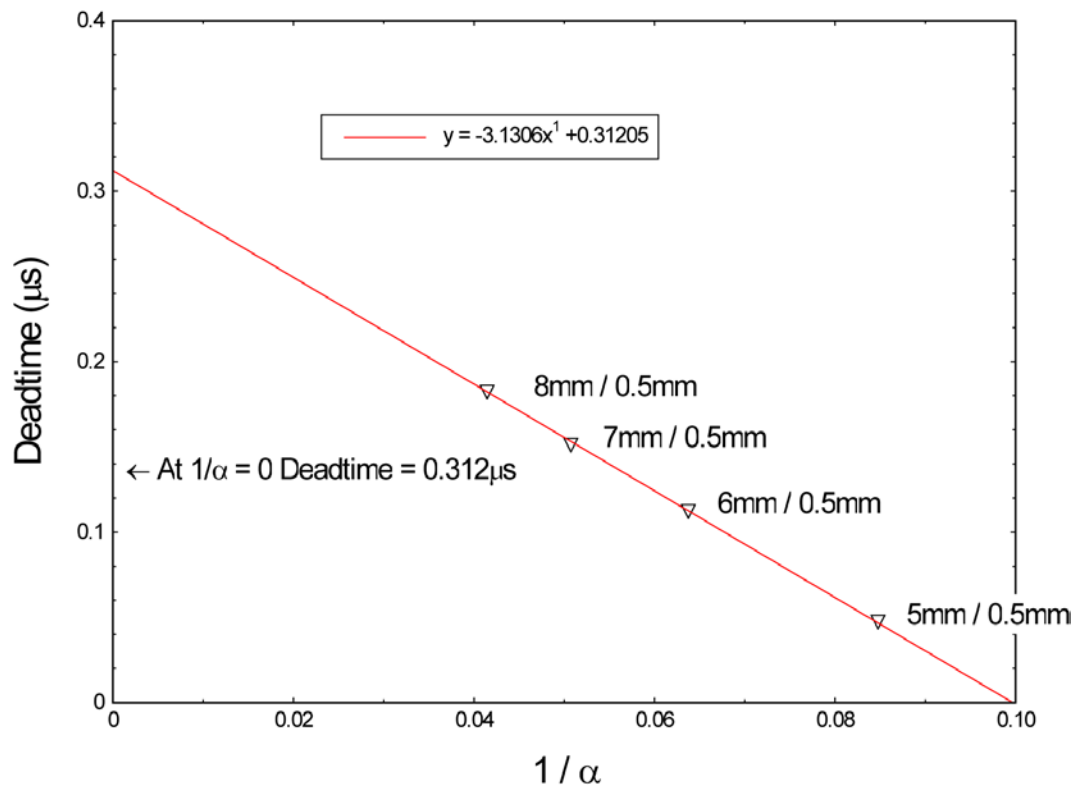
Figure 9. Plot of *b* parameter of the linear fits of Figure 8 as a function of $1/a$ (a = α)
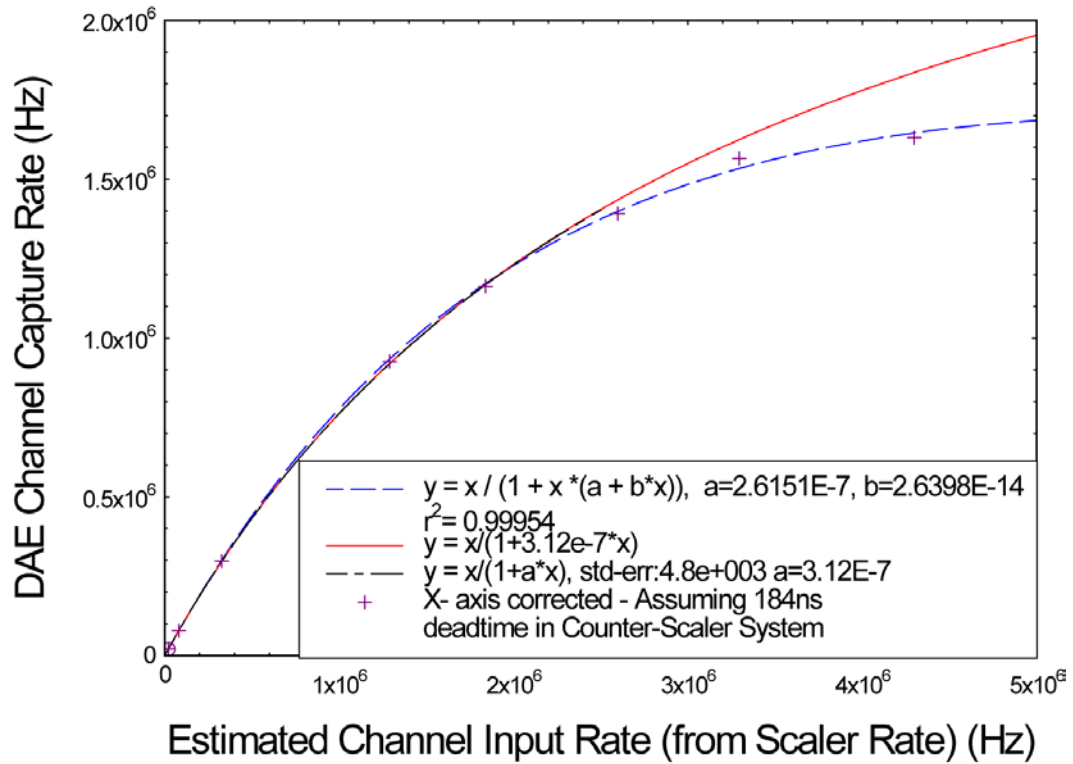
Figure 10. Estimated deadtime curve for FASTGAS using the fast scaler data
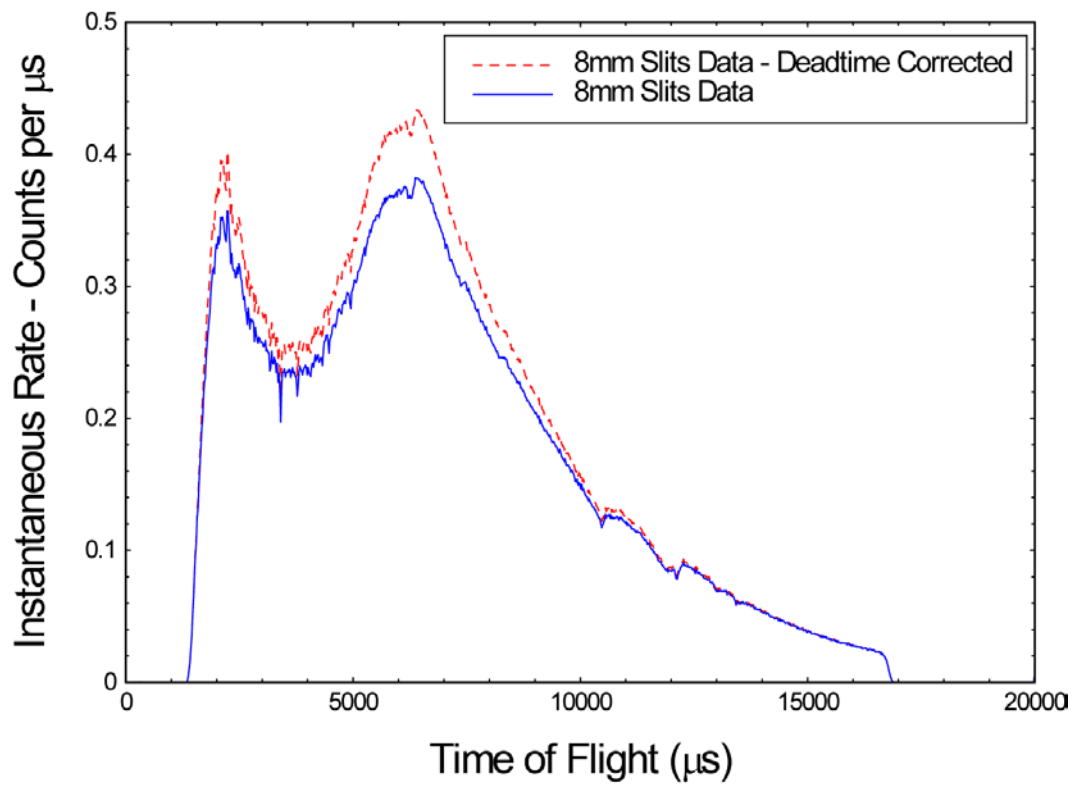
Figure 11. TOF spectrum (8mm slits) deadtime corrected using the value (312ns) deduced from Fig. 9
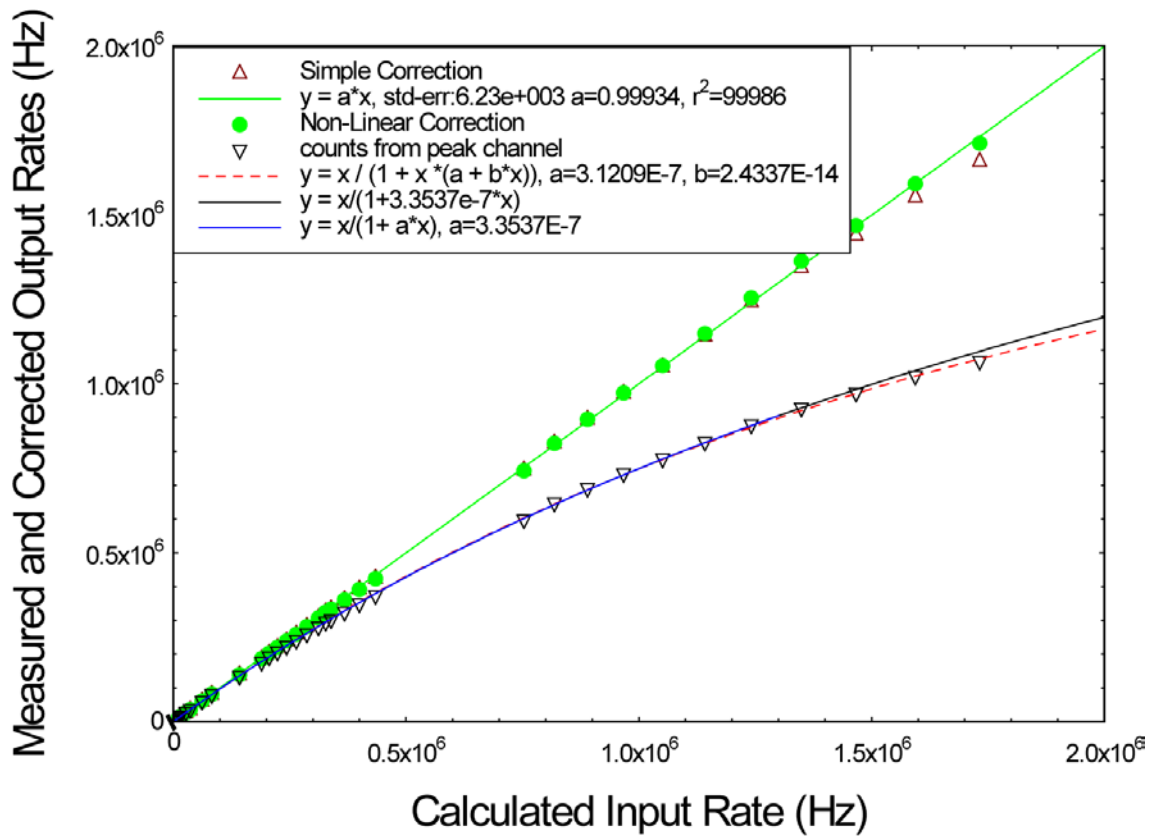
Figure 12. The data of Fig. 5 showing the non-linear fitting and correction
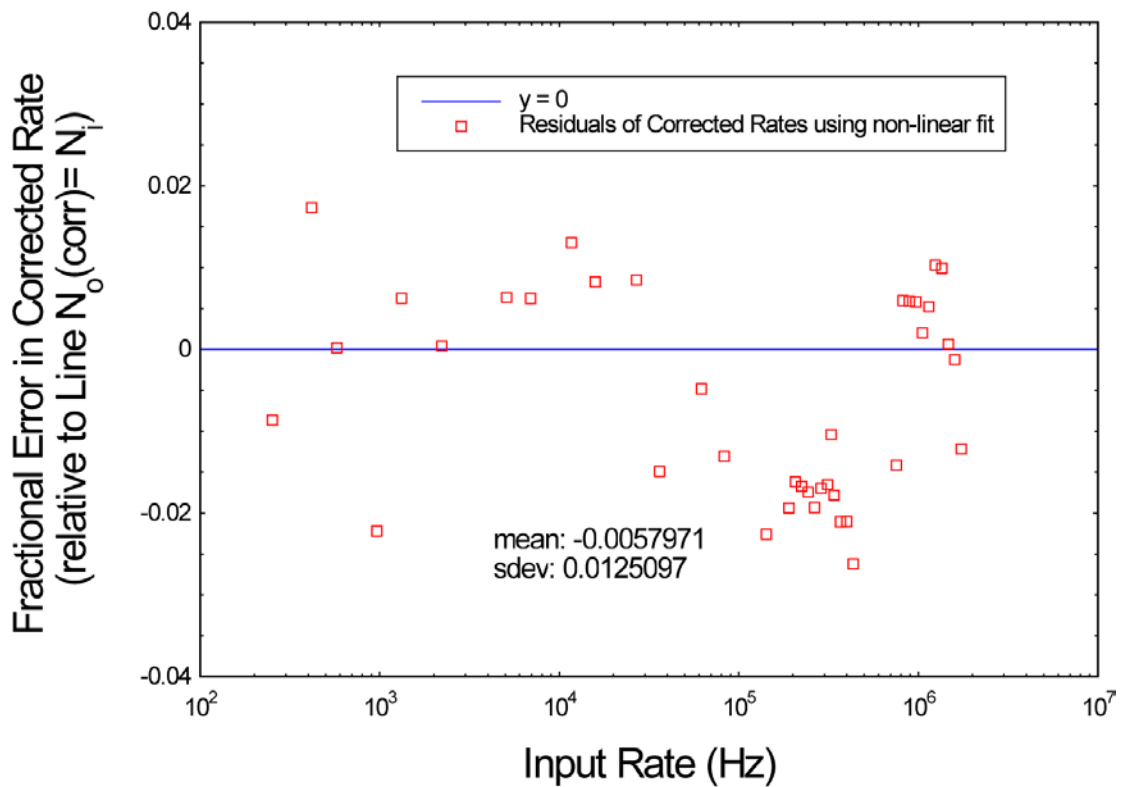
Figure 13. The fractional errors in the HOTWAXS deadtime correction (figure 12)